SEMINÁRIOS PPG-EM / UERJ 2018

PPG-EM UERJ 2018 SEMINARS

Programa de Pós-graduação em Engenharia Mecânica UERJ

SEMINÁRIOS PPG-EM / UERJ 2018

PPG-EM UERJ 2018 SEMINARS

Programa de Pós-graduação em Engenharia Mecânica UERJ

WWW.PPGEM.UERJ.BR

Capa: Imagem do dia - NASA. *"NASA Captures Supersonic Shock Interaction"*
https://www.nasa.gov/centers/armstrong/multimedia/imagegallery/Schlieren/f4_p4_red_planedrop.html

Foto dos cabeçalhos: Imagem do dia - NASA. *"GREECE Rocket Launched into the Aurora"*
https://www.nasa.gov/content/goddard/greece-rocket-launched-into-the-aurora

---

Cover: NASA Image of the day. *"NASA Captures Supersonic Shock Interaction"*
https://www.nasa.gov/centers/armstrong/multimedia/imagegallery/Schlieren/f4_p4_red_planedrop.html

Header image: NASA Image of the day. *"GREECE Rocket Launched into the Aurora"*
https://www.nasa.gov/content/goddard/greece-rocket-launched-into-the-aurora

---

April 15, 2019

Sumário / Contents

4th Seminar – November 06, 2018

5th Seminar – November 21, 2018

6th Seminar – January 09, 2019

7th Seminar – January 16, 2019

1. Introdução / Introduction

15 de Abril de 2019

O ano de 2018 foi marcado no campo científico pela perda do icônico físico inglês Stephen Hawking, mais conhecido por sua luta contra a Doença do Neurônio Motor do que por sua relevante obra no campo da física espacial. Dr. Hawking morreu em março, aos 76 anos. Sua vida chegou a inspirar a criação de um filme, lançado em 2014, contando sua história.

Sua persistência em seguir produzindo conhecimento apesar da enorme limitação física que sua doença degenerativa impunha é uma sólida fonte de inspiração para a pesquisa no Brasil de um modo geral, onde muitas vezes os recursos são escassos.

Os trabalhos reunidos neste anuário são uma demonstração de persistência dos alunos do PPG-EM da UERJ na produção científica. Foram diversos trabalhos apresentados, dos quais 10 mini-artigos foram gerados.

Agradecemos aos autores por mais um ano compartilhando seus trabalhos, expressão da persistência da Engenharia Mecânica da UERJ em fazer pesquisa.

Escrito por Leon Matos Ribeiro de Lima, doutor (2016), mestre (2010) e graduado (2007) em engenharia mecânica pela UERJ. Atualmente atua como engenheiro de processos na Eletronuclear.

April 15, 2019

The year 2018 was marked in the scientific field by the loss of iconic English physicist Stephen Hawking, better known for his fight against Motor Neuron Disease than for his outstanding work in the field of space physics. Dr. Hawking died in March at age 76. His life even inspired the creation of a movie, released in 2014, telling its story.

His persistence in continuing to produce knowledge despite the enormous physical limitations imposed by his degenerative disease is a solid source of inspiration for research in Brazil in general, where resources are often scarce.

The works gathered in this yearbook are a demonstration of the persistence of UERJ PPG-EM students in scientific production. Several papers were presented, of which 10 short papers were generated.

We thank the authors for another year sharing their work, an expression of the persistence of UERJ Mechanical Engineering in pursuing research.

Written by Leon Matos Ribeiro de Lima, doctor (2016), master (2010) and graduated (2007) in mechanical engineering by UERJ. Currently employed as process engineer at Eletronuclear.

2. Mini-artigos / Short papers

15 de Abril de 2019

Neste capítulo são apresentados os mini-artigos dos dez trabalhos científicos que fizeram parte dos Seminários do PPG-EM em 2018. Os trabalhos estão organizados segundo a data de apresentação.

Prof. Gustavo Rabello dos Anjos, D.Sc. coordenou os Seminários do PPG-EM em 2018.

April 15, 2019

This chapter presents the short papers of the ten scientific works that participated in the PPGEM Seminars in 2018. Papers are organized according to the date of presentation.

Prof. Gustavo Rabello dos Anjos, D.Sc. chaired the PPG-EM Seminars in 2018.

STRUCTURAL OPTIMIZATION USING CROSS-ENTROPY METHOD

Author: Marcos Vinicius dos Santos Issa[1] *marcosviniciusissa@gmail.com*
Advisor(s): Americo Cunha Jr[1], Francisco José da Cunha Pires Soeiro[1]
[1] State University of Rio de Janeiro

PPG-EM Seminars: season **2018**
Aug 08, 2018 www.ppg-em.uerj.br

Keywords: structural optimization, cross-entropy

1 Introduction

Structural optimization is an engineering discipline that deals with the minimization of a suitable performance function, seeking to improve the response of a mechanical system of interest. Frequently, the aim is to minimize the structure weight, respecting a suitable criteria of structural integrity. Due to complex geometric configurations and the use of advanced materials, whose behavior is extremely non-linear, this task can be too challenging, requiring the use of very efficient optimization algorithms.

This work aims to test the effectiveness and robustness of the cross-entropy (CE) method [1] , a relatively new optimization technique, in the context of structural optimization. For this purpose, a structural optimization problem that seeks to minimize the weight of a two-dimensional truss, ensuring its structural integrity, is employed as benchmark.

The rest of the paper is organized as follows. Section 2 presents the mechanical system of interest and the model equations. In section 3 the reader is introduced to the addressed structural optimization problem and the employed optimization techniques. Numerical results are presented and discussed in section 5, while final considerations are made in section 6.

2 Mathematical Model

2.1 Structural model

The structural system presented in this article was the first one where this optimization method was applied and served as motivation to apply the same method in other structural models. The structural system of interest is two-dimensional truss illustrated in Figure 1 which also show the geometric dimensions of the structure and the employed coordinate system. This truss consists of 11 bars, labeled from 1 to 11, connected through 6 nodes, labeled from 1 to 6, each one with two degrees of freedom, u_e for the horizontal displacement of bar e and v_e for the corresponding vertical displacement, where $e = 1, \cdots, 11$. These bars are made of a single material, with density $\rho = 7900\ kg/m^3$ and elastic modulus $E = 210\ GPa$. The kinematic constraints are due to the fixed support on node 1 and the roller support on node 5. Three vertical loads are applied at the nodes 2, 4 and 6, with magnitudes respectively equal to 50 kN, 100 kN and 50 kN. [2].

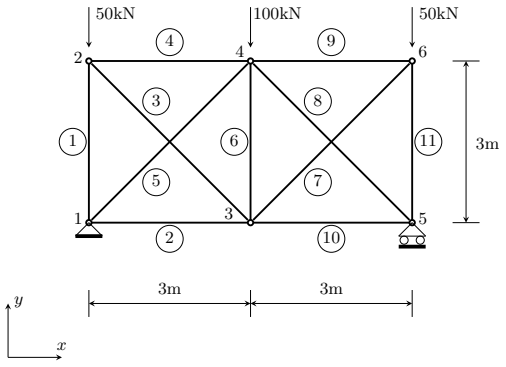

Figure 1

The equilibrium equations are obtained from the principle of virtual work, being written as the following matrix system

$$\mathbf{K}\,\mathbf{u} = \mathbf{f}\ , \tag{1}$$

where $\mathbf{K}$ is the stiffness matrix, $\mathbf{u}$ is the displacement vector and $\mathbf{f}$ is force vector.

Besides that, the stiffness matrix can be written as

$$\mathbf{K} = \sum_{e=1}^{N} \overline{\mathbf{K}}_e\ , \tag{2}$$

where $N = 11$ is the the number of bars and $\overline{\mathbf{K}}_e$ is the elementary stiffness matrix in global coordinates. In local coordinates the elementary stiffness matrix of the bar e is given by

$$\mathbf{K}_e = \frac{A_e E_e}{L_e} \begin{bmatrix} c^2 & cs & -c^2 & -cs \\ cs & s^2 & -cs & -s^2 \\ -c^2 & -cs & c^2 & cs \\ -cs & -s^2 & cs & s^2 \end{bmatrix}, \tag{3}$$

$$c = \cos\theta_e \quad and \quad s = \sin\theta_e\ .$$

where A_e is the cross-sectional area, E_e is the material modulus of elasticity, L_e is the element length and θ_e is the angle formed between the bar longitudinal axis and the horizontal axis of the reference system (x axis).

2.2 Structure mass

Each bar of the truss has a circular tubular cross-section with area is given by $A_e = \left(4\,d\,t + 4t^2\right)\,\pi/4 = \left(d\,t + t^2\right)\pi$, where d is the internal diameter and t is the section thickness. In this way, the mass of bar e is given by $m_e(d,t) = \rho\,L_e\,\left(d\,t + t^2\right)\pi$ and the total mass of the two-dimensional truss is

$$m(d,t) = \sum_{e=1}^{N} m_e(d,t) = \sum_{e=1}^{N} \rho\,L_e\,\left(d\,t + t^2\right)\pi. \qquad (4)$$

2.3 Structural integrity criterion

By Hooke's Law the normal stress at the bar e is $\sigma_e = E\,\mathbf{B}_e\,\mathbf{u}_e$, where

$$\mathbf{B}_e = \frac{1}{L_e}\left[\,-\cos\theta_e \quad -\sin\theta_e \quad \cos\theta_e \quad \sin\theta_e\,\right], \qquad (5)$$

and the local displacement $\mathbf{u}_e$ is implicitly defined by the local equilibrium equation $\mathbf{K}_e\,\mathbf{u}_e = \mathbf{f}_e$, so that the normal stress can also be written as

$$\sigma_e = E\,\mathbf{B}_e\,\mathbf{K}_e^{-1}\,\mathbf{f}_e. \qquad (6)$$

The structural integrity criterion employed here states that (in absolute value) the normal stress at each bar, defined by Eq.(6), is less than or equal to the material yield stress $S_Y = 205\ MPa$. Once σ_e depends on $\mathbf{K}$, that depends on $A_e(d_i,t)$, the normal stress is a function of d_i and t and the integrity criterion can be written as

$$|\sigma_e(d_i,t)| - S_y \le 0, \qquad e = 1,\cdots,N. \qquad (7)$$

Another criterion is buckling load (Euler Critical Load)

$$\sigma_{E_e} = \frac{\pi^2 E I_e}{L_e^2 A_e}\,, \qquad (8)$$

where I_e is inertial moment.

3 Structural optimization problem

The structural optimization problem considered here aims to minimize the structure mass, Eq.(4), using d and t as design variables, considering as constraints the inequalities in (7), and a limited set of values for d and t, i.e.,

$$d_{min} \le d \le d_{max} \qquad \text{and} \qquad t_{min} \le t \le t_{max}. \qquad (9)$$

4 Solution algorithms

Three different optimization techniques are employed in this work to deal with the nonlinear optimization problem : (i) sequential quadratic programming (SQP), (ii) genetic algorithm (GA), and (iii) cross-entropy (CE) method.

SQP and GA are well-known methods in the structural optimization community. The three methods will not be described for lack of space, but that can be studied in the references [3], [4] and [1].

5 Optimization Experiments

In order to evaluate CE accuracy, a comparison with the reference results obtained via SPQ and GA is done in Table 5.

Method	mass(kg)	$d^\star$(mm)	$t^\star$(mm)	time*(sec)
SQP	288	56.2	5.0	0.6
GA	293	55.9	5.1	10.7
CE	293	55.9	5.1	3.0

*Dell Inspiron i15 7559-A30 "Core i7" 2.8 GHz 16GB 1600 MHz DDR3L

Illustration of CE (5 sampling of the domain at different levels (iterations). The red cross is the SPQ reference solution, and the magenta cross corresponds to CE solution.

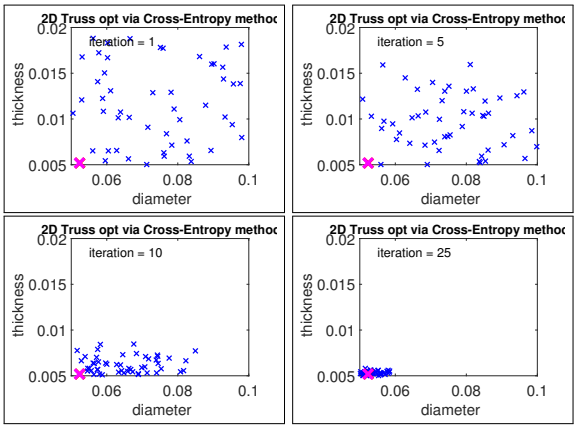

6 Conclusions

This work addresses a numerical study evaluating the effectiveness and robustness of the cross-entropy method in the context of structural optimization. The results show that the evaluated method is very competitive, having a much better performance than genetic algorithm in terms of processing time. In comparison to the sequential quadratic programming, cross-entropy has comparable processing time, proving to be a very appealing tool for optimization problems, especially when the use of gradients is impractical.

7 Acknowledgments

The author thanks FAPERJ for the financial support.

References

[1] D. P. Kroese, R. Y. Rubinstein, I. Cohen, S. Porotsky and T. Taimre, Cross-Entropy Method, In *Encyclopedia of Operations Research and Management Science*, edited by S. I. Gass and M. C. Fu, pages 326-333, Springer, 2013. http://dx.doi.org/10.1007/978-1-4419-1153-7_131

[2] A. J. M. Ferreira, MATLAB Codes for Finite Element Analysis Solids and Structures, Springer, 2009.

[3] J.F. Bonnans, J. C. Gilbert, C. Lemarechal and C. A. Sagastizábal, Numerical Optimization: Theoretical and Practical Aspects, Springer, 2nd edition, 2009.

[4] O. Kramer, Genetic Algorithm Essentials, Springer, 2017.

CHARACTERIZATION OF FLY ASHES BY BRAZILIAN THERMOELECTRIC POWER PLANTS

Author: Diego de Lima Gomes[1] *diego.lima@uerj.br*
Advisor(s): Marilia Diniz[1]
[1] State University of Rio de Janeiro

PPG-EM Seminars: season **2018**
Aug 15, 2018 www.ppg-em.uerj.br

Keywords: Mineral coal, fly ash, characterization, microhardness.

1 Introduction

In thermoelectric power generation that uses mineral coal as fuel, the basic mechanism of deterioration of pipes and metallic equipment in boilers are formed by three combined factors: erosion-corrosion-high temperatures. This deterioration has technical-economic implications for power plants. The main erosion agent are the fly ash particles, composed by coal combustion products that collide with the surfaces of boiler components. The damage caused are not limited to the cost for replace components, but also to the cost of shutting down energy production and the risks involved with equipment operating at hight temperatures. The use of coal as fuel in thermal energy sources produces a large amount of solid waste classified as ash. Only Brazil is responsible for generating about 3 million tons of annual ash, with 80 % of waste being fly ash [1-4].

2 Materials and Methods

Samples of the ash was collected from the residue of mineral coal-fired used as fuel to generate steam in a boiler of a thermoelectric plant in operation located in the South region of Brazil, as agent that causes the possible mechanism of equipment wear. Were used metallographic preparation techniques, pH evaluation, scanning electron microscopy (SEM), semi-quantitative chemical analysis by energy dispersive spectroscopy (EDS), quantitative determination of elements by gravimetric analysis and atomic absorption spectrophotometry, Transmission electron microscopy (TEM) and Vickers microhardness measurements (HV).

2.1 pH evaluation

The ash particles were diluted in distilled and deionized water to measure their potential of hydrogen (pH) to indicate the degree of acidity of material. An Omega PHH7000 pHmeter was used. The extract consisted of 50.08 g of the ash sample and 250.07 g of water. The test occurred at a temperature of 23 $\pm$ 2 $^{\circ}$ C.

2.2 Scanning Electron Microscopy (SEM)

To obtain high resolution images of ash particles, a scanning electron microscope (SEM) with secondary electron detector (SEI) model JEOL JSM 6510-LV used at 20kV was used.

2.3 Gravimetric analysis and atomic absorption spectrophotometry

The tests for verification of element contents were used for the following procedures:

- Determination of silicon by gravimetric of atomic absorption;

- Determination of metals in solution by atomic absorption spectrophotometry.

2.4 Transmission electron microscopy (TEM)

Some ash particles were observed through a transmission electron microscope (TEM / STEM) model JEOL 2100F operated at 200 kV, equipped with an EDS detector, able to obtain images by bright field (BF) and dark field (DF), diffraction contrast and elemental mapping.

2.5 Microhardness measurements

Values of Vickers microhardness (HV) were obtained for individual particles by a microdurometer model PANTEC MV-1000A, using a load of 0.9807 N in a time of 15 seconds of application.

3 Results

Analysis by microscopy techniques allowed the study of the structure and morphology of fly ashes particles Figure 1. The pH evaluation revealed a hight alkalinity (pH = 9.4). The indicators for potential of hydrogen should be considered when the residue contain presence of humidity or water. The alkalinity presented in the sample can promote chemical protection to steel and protect against corrosion. The morphological aspect of the particles showed a predominantly spherical with varied diameters and a few particles of irregular forms (elliptical and acicular) Figure 2. This morphological

aspect is totally in agreement with the literature [5].

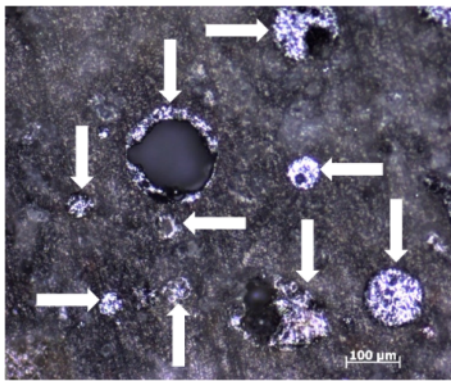

Figure 1: Ash particles embedded in acrylic resin after metallographic preparation. OM, 100x.

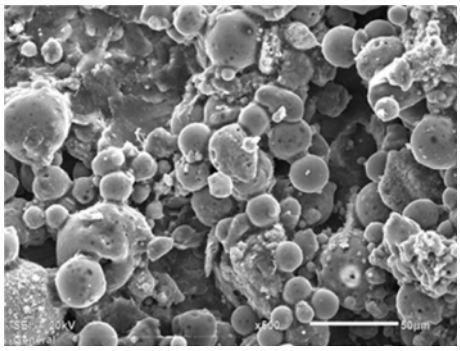

Figure 2: Appearance of coal fly ash particles. SEM, 500x.

The results obtained by the EDS analysis of the sample and the characterization by atomic absorption spectrophotometry showed significant levels of silicon, iron and aluminum elements.

Analysis of size distribution showed that most of the ash composition consists of particles from 5 to 45 μm, relative of 68% of the analyzed particles. This confirmed the treatment by fly ashes for the particles.

The TEM/STEM analyzes collaborated for the chemical evaluation of sample. Once again no sulfur were identified. Figure 3.

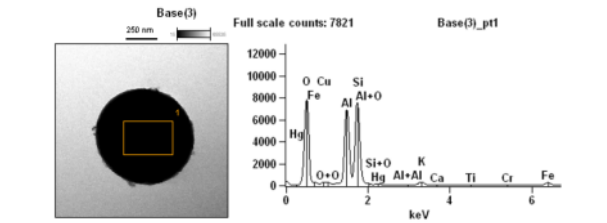

	O-K	Al-K	Si-K	K-K	Ca-K	Ti-K	Cr-K	Fe-K
Base(3)_pt1	59.394	17.690	22.019	0.389	0.049	0.012	0.009	0.067

Figure 3: Chemical analysis of fly ash particle STEM mode.

It is noticed a large percentage of silicon and aluminum in the particle, which is in agreement with other results found.

Hardness measurements were performed on several individual particles. As mechanical property, hardness is used in the specification and comparison between materials. There is great difficulty in obtaining this parameter of measurement in hardness particles with micrometric scale dimensions. The value found was close to that indicated in the literature for quartz from 900 - 1280 HV.

4 Conclusions

After the chemical, geometric and dimensional characterization of the particles, it was possible to conclude that the ash particles had a predominantly spherical morphological aspect of various diameters, with a combination mainly of aluminum, silicon and iron oxide and basic characteristics indicator. Particles were observed with solid elements and others with internal voids as well particles of irregular shapes. The mean hardness value by the sample was similar to found for quartz. The results presented will contribute greatly to the future development of coatings for the protection of pipes and systems that occurs wear caused by the impact of coal ash in boilers of thermoelectric power plants.

5 Acknowledgments

The author would like to give a special thanks for the advisor of this research Marilia Diniz, the research group of CEPEL and laboratories of PUC-RJ and CBPF for support in this research work.

References

[1] Sundstron, M. G., “Caracterização e avaliação das cinzas da combustão de carvão mineral geradas na região do baixo Jacií - RS” (2012).

[2] Schaeffer. L., “Estudo de propriedades de alumínio reforçado 50 % de carga de cinza leve proveniente da queima de carvão termoeletrico” (2013).

[3] Goodarzi, F., “Characteristics and composition of fly ash from Canadian coal-fired power plants” (2006).

[4] Bortoluzzi, R. L., “Estudo da erosão por cinza volante em diferentes tipos de ligas de aço aplicadas em caldeira de grande porte” (2015).

[5] Desale, G. R., “Effect of erodent properties on erosion wear of ductile type materials” (2006).

WEB SYSTEM FOR WEATHER DATA PROCESSING TO HVAC DESIGN

Author: Raama Costa Alves[1] *raama.costa@gmail.com*
Advisor(s): Manoel Antonio da Fonseca Costa Filho[1]
[1] State University of Rio de Janeiro

August 15, 2018
PPG-EM Seminars: season **2018**
www.ppg-em.uerj.br

Keywords: data processing, climate data, software,weather data, air conditioning.

1 Introduction

The usage of most accurate weather data enables to reduce safety factors in heating, ventilating and air conditioning (HVAC) designs, resulting in better HVAC dimensioning and consequently reducing operational costs and saving energy. The last is one of the main priorities in the building sector.

The Brazilian air conditioning design standard NBR-16401 [2] follows the meteorological data processing method from ASHRAE 2013 [3] and provides climatic data for only 34 Brazilian cities. For other cities, it defines criteria to find among the cities listed, that whose climatic parameters are the closest to the project city, known as the corresponding city. However, the extent of Brazilian territory and the vast climatic diversity suggest the need to obtain specific weather data for each location.

This work aims at presenting a web system named DwpGen for weather data processing to HVAC design, following the criteria established by ASHRAE. Design data for cooling and dehumidification for a Brazilian city was calculated and compared with its corresponding city.

For an American city design data was calculated and compared with design data supplied by ASHRAE.

2 Materials and Methods

An application development involves many steps and plays an essential role to determine the database schema requirements.

In this work criteria related to scalability, availability and price of hosting platforms were also taken into account to choose PostgreSQL as the database management system [5].

For the web system developmen, PHP programming language was selected because it is multiplatform, robust, rapid, free and easy-learning [4].

2.1 Study cases

The selected city come from Brazilian bioclimatic zones according to the Brazilian standard NBR 15220-3 [1]. Its weather data were supplied by the Instituto Nacional de Meteorologia (INMET). Table 1 shows yearly data available and the corresponding city in the Brazilian standard.

An American city presented in ASHRAE (2013) was chosen to validate this Web System. Their weather data was supplied by the National Centers for Environmental Information (NCEI). Table 2 shows the following information about the city.

City	Data Avaiable	Corresponding City
Itiruçú/BA	2003-2016	Goiânia/GO

Table 1: Chosen Brazilian City.

City	Data Avaiable
Tampa/Florida	1986-2010

Table 2: Chosen American City.

2.2 Data Processing

The temperature frequency distributions were built as described below:

Step 1. Import the weather data to the DwpGen database;

Step 2. Discard any month will if the sum of the dry bulb temperature (DBT) empty intervals greater than 6 hours overcome 15% of the total month hours. Fill DBT and dew point temperature (DPT) gaps by linear interpolation for intervals less or equals to 6 hours.

Step 3. Discard any month if the difference between total diurnal and nocturnal hours is greater than 60.

Step 4. Discard any month if the sum of empty DPT values overcomes 15% of the total DBT available, except when relative humidity (RH) hourly data are supplied. Fill DPT gaps using simultaneous DBT and RH values through psychometrics equations and repeat the step 3.

Step 5. Create a database with the same number of

repetitions for all months eliminating the exceeding oldest ones for a minimum of eight years, otherwise the database available is not complete enough for continuing. Compute the design DBT and DPT for the desired frequency levels;

Step 6. Compute the average daily temperature range only for the hottest month and re-organize the database in decreasing order of DBT and find the points corresponding to the desired frequency levels;

Step 7. Find the coincident wet bulb temperature (cWBT) by averaging the simultaneous WBT values with the corresponding design DBT determined in the step 6.

Daily temperature profiles for the design day were calculated as described in ABNT [2].

3 Results

Figue 1 shows the cooling and dehumidification design data for Itiruçú and the design data reproduced from ABNT (2008) for its corresponding city, Goiânia.

City	Annual Frequency Level					
	0.4%		1%		2%	
	DBT	WBTc	DBT	WBTc	DBT	WBTc
Itiruçu	31.3	19.8	30.3	19.9	29.4	19.7
Goiânia	35	20.3	34	20.7	33.1	20.8

Figure 1: Design Data calculated for Itiruçu and for Goiânia from ABNT (2008)

Figure 2 shows that the hourly DBT profile from Itiruçu is always below that from Goiânia. Therefore, it is important to evaluate the behavior of the thermal load for the design at Itiriçu to avoid oversizing of the air conditioning system.

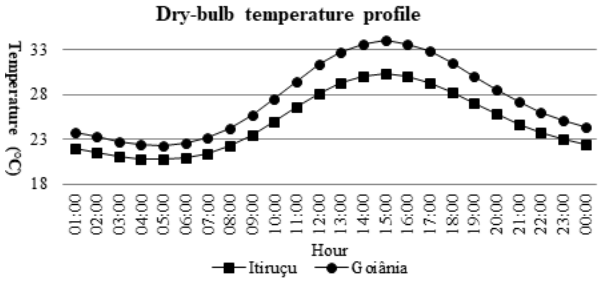

Figure 2: Hourly dry-bulb temperature profile at 1% frequency level - Itiruçu and Goiânia

Figure 3 shows the cooling and dehumidification design data calculated for Tampa and design data reproduced from ASHRAE (2013).

City	Annual Frequency Level					
	0.4%		1%		2%	
	DBT	WBTc	DBT	WBTc	DBT	WBTc
Tampa	33.9	25	32.8	25.1	32.2	25
Tampa (ASHRAE)	33.6	25.1	33	25.1	32.4	25.1

Figure 3: Data calculated and design data from reproduced from ASHRAE (2013) for Tampa

Figure 4 shows for Tampa, at 1% frequency level, the hourly dry bulb temperature profiles for the design day supplied by ASHRAE and calculated by DwpGen.

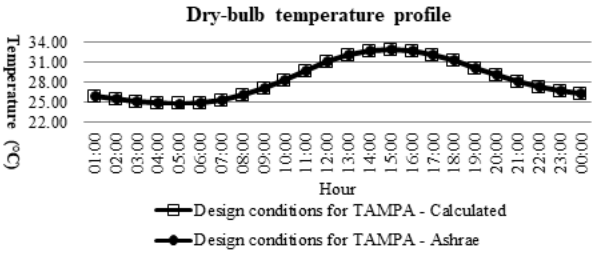

Figure 4: Hourly dry-bulb temperature profile at 1% frequency level - Tampa

4 Conclusions

The use of DwpGen allows to determine the design parameters for cooling and dehumidification systems for any Brazilian locality based on hourly weather data organized as those provided by the INMET. This tool will enable the designer to perform an accurate analysis of the climatic conditions of the locality where the system will be installed.

The DwpGen was validated through comparison with data presented in ASHRAE (2013) and the results were satisfactory. Better agreement could be achieved if the meteorological data periods for processing were the same.

Import tools for weather data types other than those from INMET are under development. The program is growing in functionalities and soon will be able to generate Typical Meteorological Year files as requested for simulation performance of the HVAC systems.

References

[1] ABNT. *Associação Brasileira de Normas Técnicas - NBR 15220-3: Desempenho térmico das edificações - Zoneamento bioclimático brasileiro e diretrizes construtivas para habitações unifamiliares de interesse social*. 2005.

[2] ABNT. *Associação Brasileira de Normas Técnicas - NBR 16401-1: Instalações de Ar-condicionado – Sistemas Centrais e Unitários. Parte 1: Projeto das instalações*. 2008.

[3] ASHRAE. *American Society of Heating, Refrigerating, and Air-Conditioning Engineers – Handbook Fundamentals. Chapter.14. Climatic Design Information*. 2013.

[4] Dall'Oglio, P. *PHP Programando com Orientação a Objetos*. 2015.

[5] Empresa Brasileira de Pesquisa Agropecuária. Utilizando o formato JSON para armazenar dados do sistema BDGF no PostgreSQL. https://www.infoteca.cnptia.embrapa.br/infoteca/bitstream/doc/1065251/1/Doc151.pdf, 2016. Online; accessed 20 March 2018.

USING ORGANIC RANKINE CYCLE FOR ELECTRICITY GENERATION FROM WASTE HEAT

Author: Valmir de Oliveira Jr[1] *valmir.deoliveira@gmail.com*
Advisor(s): Manoel Antonio da Fonseca Costa Filho[1]
[1] State University of Rio de Janeiro

PPG-EM Seminars: season **2018**
www.ppg-em.uerj.br
Oct 31, 2018

Keywords: Organic Rankine Cycle, waste heat, energy efficiency.

1 Introduction

The Organic Rankine Cycle (ORC) operates similarly to a steam Rankine cycle with the same components, replacing the water by organic fluids with high molecular mass which have lower boiling points. This enables thermal recovery from milder temperature sources, being suitable for electricity generation from solar, geothermal, biomass and residual heat sources. The waste heat in exhaust gas from internal combustion engines corresponds to approximately 55% of the total heat released by the fuel. The thermodynamic model for each component of the cycle is based on the mass and energy balances and was done using the software Engineering Equation Solver (EES) from the F-Chart Software..

2 Working Fluids Candidates

The choice of working fluid, which alternately vaporizes and condenses when it absorbs and releases thermal energy, is the main part for the sizing of the cycle. Most often, it is necessary to make a comparison between a set of possible candidate fluids in terms of thermodynamic performance and based on the final purpose of the cycle.

According to [3], o fluid needs to have specific characteristics depending on the application, for instance: appropriate saturation temperature, low critical pressure and temperature, reduced specific volume, low viscosity and surface tension, high thermal conductivity, non-corrosive and toxic, compatibility with turbine material, if appropriate with national and global environmental laws.

3 Methods

The current investigation was made on the marine propulsion diesel engine Caterpillar 3516C which characteristics are presented in Tab. 1.

Table 2 presents a pre-selection of the working fluids to be tested. It was made in accordance with [4] that summarizes the scientific literature in the field of working fluid selection for ORC systems. After comparing several studies, those authors took in account three characteristics: the target application and the desired ranges of the condensing and evaporating

Parameter	Specification
Engine type	V-16, Diesel
Engine Heat to Atm. (kW)	149
Exhaust Flow, $\dot{m}_{exh}$ (m^3/min)	53.9
Exhaust Temp., T_{exh} (^{o}C)	501.8

Table 1: Diesel Engine Technical Specifications.

Fluids		
R113	R123	R236ea
Benzene	n-Pentane	R11
Toluene	R245fa	R141b

Table 2: Working Fluid Pre-Selection.

The thermodynamic model for each component of the cycle is based on the mass and energy balances. All thermodynamic property ranges were limited to practical design constraints imposed to each equipment, such as obeying the minimum pinch points in the heat exchanger designs.

The Engineering Equation Solver was used for thermodynamic modeling of the company F-Chart (www.fchart.com). EES is a general equation-solving program that can numerically solve thousands of coupled non-linear algebraic and differential equations. A major feature of EES is the high accuracy thermodynamic and transport property database that is provided for hundreds of substances in a manner that allows it to be used with the equation solving capability.

The pinch point temperature difference (PPTD) corresponds here to the minimum difference between the exhaust gas temperature and the temperature organic fluid evaporating temperature.

Figure 1 shows temperature-heat exchanger path length for counterflow (steam generators). The minimum approach point between the two lines is the PPTD, represented by b-B.

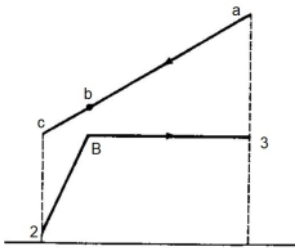

Figure 1: Temperature-heat exchanger path length diagram for the boiler

4 Results

In this study, due to the high temperature of the exhaust gases, it was necessary to perform the modeling of two types of ORC (ideal and regenerative), for all the fluids suggested by [4] and shown in Tab. 2.

The variations of some parameters say a lot about the efficiency of a cycle Rankine, the same happens in an organic cycle, so from the variation of the mass flow of the organic fluids in the ideal and regenerative cycles, in the thermodynamic equations, graphs can be elaborated of the behavior of the substances in relation to the efficiency, for the motor and the type of ORC, in agreement with the images below:

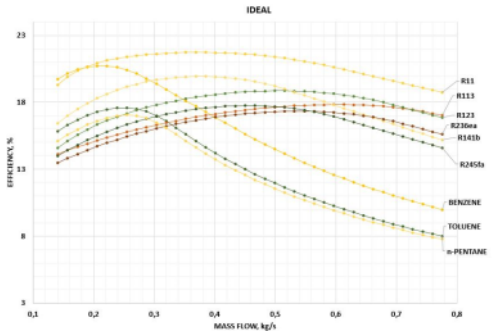

Figure 2: Effect of organic fluid mass flow on cycle idal

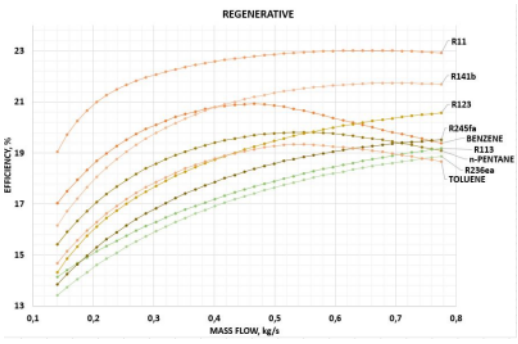

Figure 3: Effect of organic fluid mass flow on cycle regenerative

Some fluids were discarded after modeling the whole systems, since they did not present the expected result in relation to cycle efficiency, condensation and evaporation temperatures, and restriction of 10K as PPTD in the boiler. The fluids that have presented the best performances were chosen as suitable work fluids: Benzene, Toluene and n-Pentane.

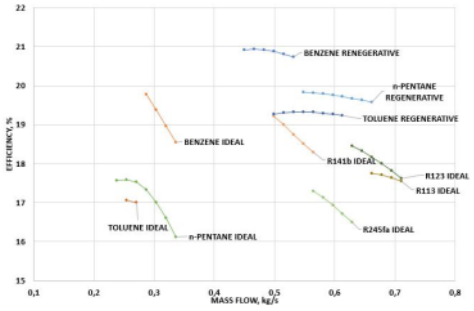

Figure 4: Effect of organic fluid mass flow on cycle regenerative

5 Conclusions

It was proposed the elaboration of an organic Rankine cycle model for electricity generation from residual heat recovery of the Caterpillar diesel engine with the help of EES software.

Several work fluids recommended in the scientific literature were tested, in which the difference in behavior can be observed.

Since the graphs of the fluid behavior with the determined pressures were determined, limiting the PPTD and without suffering overheating, it was found that Benzene, Toluene and n-Pentane present good yields, with Benzene providing the highest amount of heat recovery 31.11 kW, corresponding to 1.23% of the engine braking power.

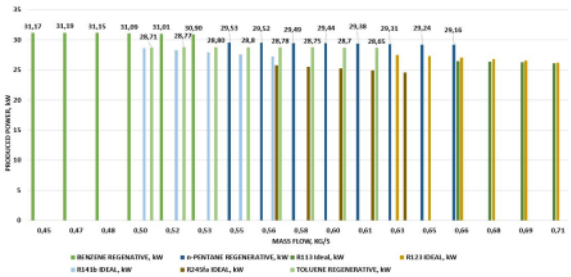

Figure 5: Power produced in kW by the ORC with working fluids

References

[1] Yunus A Çengel and Michael A Boles. *Termodinamica*. McGraw Hill, 8 edition, 2015.

[2] Mohamed Mohamed El-Wakil. *Powerplant Technology*. Tata McGraw-Hill Education, 1984.

[3] Hao Liu, Yingjuan Shao, and Jinxing Li. A biomass-fired micro-scale chp system with organic rankine cycle (orc)–thermodynamic modelling studies. *Biomass and Bioenergy*, 35(9):3985–3994, 2011.

[4] Sylvain Quoilin. *Sustainable energy conversion through the use of organic Rankine cycles for waste heat recovery and solar applications*. PhD thesis, University of Liege, Belgium, 2011.

REAGENT ADDITION SPEED STUDY IN THE SYNTHESIS OF HYDROXIAPATITA BY THE SOL-GEL METHOD USING CASES OF CHICKEN EGGS AS PRECURSORS

Author: Adilson Quizunda[1] *adyquizunda@hotmail.com*
Advisor(s): José Brant[1]
[1] State University of Rio de Janeiro

PPG-EM Seminars: season **2018**
www.ppg-em.uerj.br
Nov 6, 2018

Keywords: Reagent, Speed, Addition, Hydroxiapatita.

1 Introduction

The formula for the stoichiometric hydroxyapatite is Ca10 (PO4) 6 (OH) 2, Ca / P ratio equal to 1.67 and is the most stable and least soluble calcium phosphate. It is one of the most attractive materials for commercial use due to its wide application in various fields, such as: bone and dental implants; catalyst; support for catalysts, fertilizers and effluent treatment. According to the synthesis method (sol-gel, hydrothermal treatment, with microwave irradiation, or melting solid precursors at high temperatures) used for the production of Hydroxyapatite (Hap), different types of material will be obtained with different applications [1].

2 Objective

The objective of this work is to suggest the use of chicken eggshell as sources of calcium for the synthesis of hydroxyapatite by the sol-gel method conjugated to the thermal treatment of products precipitated in the aqueous medium, using the slow and rapid addition of phosphoric acid in the reaction to obtain reuse of hydroxyapatite, the reuse of a residue (chicken eggshell) which is disposed of in landfills in a high economic value product, any efforts to reduce untreated waste discharge, reduce greenhouse gas emissions , contamination of groundwater and release of pathogens and phytotoxicants into the environment.

3 Materials and Methods

For this work a mechanical stirrer was used to keep the solution in constant agitation, a peristaltic pump, for the addition of phosphoric acid, and the addition time was monitored. The method used was sol - gel, also known as the modified Rathje method.

Egg shells -> calcination -> hydrolysis -> Ca(OH)2

10Ca(OH)2 + 6 H3PO4 -> Ca10(PO4)6(OH) + 18H2O
Ca10(PO4)6(OH) -> calcination -> characterization

4 Results

Addition of H3PO4 at the velocity of 5mL/min – slow – standard:

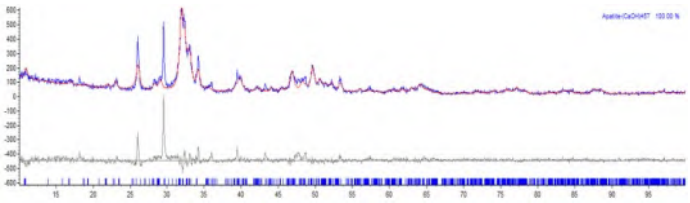

Figure 1: Diffractogram of the sample with slow addition of phosphoric acid

Addition of H3PO4 at the velocity of 20mL/min – fast:

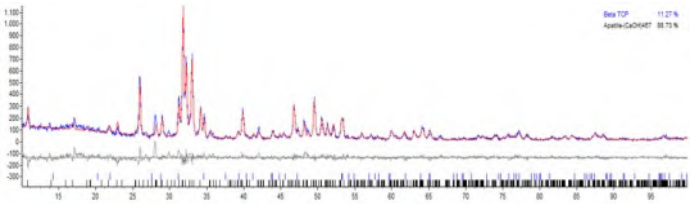

Figure 2: Diffractogram of the sample with fast addition of phosphoric acid

Scanning electron microscopy - magnification 20000x:

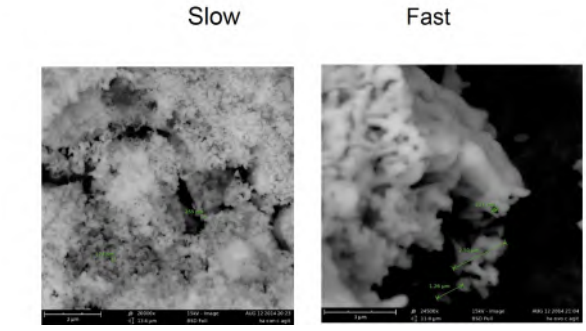

Figure 3: SEM image with magnification of 20000x

5 Conclusions

The obtaining of stoichiometric powders of HAp depends on the rate of addition of the phosphoric acid that interferes in the formation of the phases, since the pH of the medium is rational and altered.

6 Acknowledgments

This work was carried out with the support of the Coordination of Improvement of Higher Education Personnel - Brazil (CAPES) - Financing Code 001 Apoio do Research and productivity program of the Estácio de Sá University.

References

[1] A.C. F. M. Costa; M. G. Lima; L. H. M. A. Lima; V. V. Cordeiro; K. M. S. Viana; C.V. Souza1; H. L. Lira. Hidroxiapatita: Obtenção, caracterização e aplicações, Campina Grande, 2010, 10f, artigo.(Universidade Federal de Campina Grande).

[2] Fook, A.C.B.M.I; Aparecida, A.H.II; Fook, M.V.L. ''Desenvolvimento de biocerâmicas porosas de hidroxiapatita para utilização como scaffolds para regeneração óssea", Campina Grande, 2010, 8f, artigo.(Universidade Federal de Campina Grande).

[3] Leite, R.B.1, Araújo, P.M.A.G., Nepomuceno, F.G., Santos, P.T.A., Costa, A.C.F.M. Hidroxiapatita por reação de combustão para aplicação ortopédica, Campina Grande, 2017, 9f, artigo (Dep. De Engenharia de Materiais, Universidade Federal de Campina Grande, Campina Grande , Brasil).

BLOOD FLOW NUMERICAL SIMULATION USING FINITE ELEMENT METHOD IN A STREAM-VORTICITY FORMULATION WITH TAYLOR-GALERKIN SCHEME

Author: Leandro Marques[1] *marquesleandro67@gmail.com*
Advisor(s): Gustavo Anjos and Jose Pontes[1]
[1] Rio de Janeiro State University

PPG-EM Seminars: season **2018**
www.ppg-em.uerj.br
Nov 21, 2018

Keywords: Stream-Vorticity Formulation, Finite Element Method, Taylor-Galerkin Scheme, Drug-Eluting Stent.

1 Introduction

According to the World Health Organization [7], more people die annually from the cardiovascular disease (CVD) that from any other cause in the world and the percutaneous transluminal coronary angioplasty (PTCA) treatments, with drug-eluting stent placement, is being performed to help solve this problem. This work aims to develop a 2D Finite Element code for stream-vorticity formulation with species transport equation using Taylor-Galerkin scheme, besides to know how occurs the dynamics of blood flow in coronary artery with atherosclerosis and with stents struts placed.

The equations that govern the dynamics of blood flow in a coronary artery were developed according to continuum media assumption. The blood was modeled as single-phase, incompressible and newtonian fluid, the diffusion coefficient was considered as constant. The Navier-Stokes equation is shown according to the stream-vorticity formulation with species transport equation in a Finite Element Method approach.

The domain was discretized on an unstructured linear triangular mesh using the *GMSH* open source as suggested by Geuzaine and Remacle [3]. The equations were discretized in time by Taylor series expansion remaining the second order terms and the Galerkin formulation was used to discretize in space. The linear system of equations is solved throught iterative method *Conjugate Gradient Solver*. The dynamics of blood flow was investigated in a case proposed by Wang et al. [6] and the simulation was shown using *Paraview* open source as suggested by Henderson [4].

2 Mathematical Model

The governing equations were developed according to continuum media assumption, thus the universal conservation laws were used. The blood was modeled as single-phase, incompressible and newtonian fluid, the diffusion coefficiente was considered as constant, then the Navier-Stokes equation was used according to stream-vorticity formulation with species transport equation.

The domain was discretized on an unstructured linear triangular mesh using the *GMSH* open source. The equations were discretized in time by Taylor series expansion remaining the second order terms and the Galerkin formulation was used to discretize in space. Therefore, the Taylor-Galerkin scheme was used as proposed by Donea [2]. The governing equations in matrix form used in this paper were:

$$\left[\frac{M}{\Delta t} + \frac{1}{Re}K\right]\omega^{n+1} = \left[\frac{M}{\Delta t} - \mathbf{v}\cdot G - \mathbf{v}\cdot K_s\right]\omega^{n} \quad (1)$$

$$K\psi = M\omega \quad (2)$$

$$Mu = G_y\psi \quad (3)$$

$$Mv = -G_x\psi \quad (4)$$

$$\left[\frac{M}{\Delta t} + \frac{1}{ReSc}K\right]c^{n+1} = \left[\frac{M}{\Delta t} - \mathbf{v}\cdot G - \mathbf{v}\cdot K_s\right]c^{n} \quad (5)$$

where, ω is the vorticity field, ψ is the stream function field, c is the concentration field, u and v are the velocity components, $Re = \rho u D/\mu$ is the Reynolds number, $Sc = \nu/D$ is the Schmidt number. M is mass matrix, G, G_x and G_y are gradient matrix, K is stiffness matrix and K_s is stabilization matrix, it decreases the spurious oscillations as seen for moderate to high Reynolds numbers. The superscript $n+1$ is the scalar that will be calculated in currente time step and the superscript n was calculated in the previous time step.

3 Results and Discussion

The linear system of equations that comes from implementing the FEM is solved throught iterative method *Conjugate Gradient Solver* available in the public library for scientific tools *SciPy*. The dynamics of blood flow and species transport in coronary artery was investigated in a case proposed by Wang et al. [6] and shown in Figure 1, however modified for cartesian coordinates. The lumen radius of a typical artery is about $R = 0.0015$m, viscosity in the lumen are set to $\mu = 0.0035$Pa.s. and density $\rho = 1060$kg/m^3 as suggested by Bozsak et al. [1]. According to Kessler

et al. [5], the velocity of the flow at coronary artery is $v = 12$cm/s. Therefore, the Reynolds number is $Re = 54.5$ and the Schmidt number used was $Sc = 10$. According to symmetry on y coordinate, half domain was simulated and the simulation was shown using *Paraview* open source.

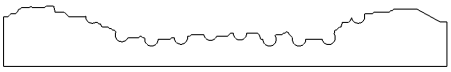

Figure 1: Real Channel with Stent.

The boundaries conditions used were: (a) *inflow condition*: $u = 0$, $v = 1$ and $\psi = y$. (b) *no-slip condition*: $u = 0$, $v = 0$ and $\psi = 1$. (c) *outflow condition*: no value is specified. (d) *free-slip condition*: $v = 0$ and $\psi = 0$. (e) *stent condition*: $u = 0$, $v = 0$ $\psi = 1$ and $c = 1$.

The geometry was taken using image processing from a real coronary artery photography. The stent is modeled by 10 semi-circles uniformely spaced and the geometry used promotes a reduction of length between the bottom and top plates when were considered 40% of channel obstruction due to atherosclerosis. The Figure 2 shown velocity field profile evolution along y coordinates in centerline ($x = 5R$). As can seen, the maximum u-velocity is nearly three times the nominal value.

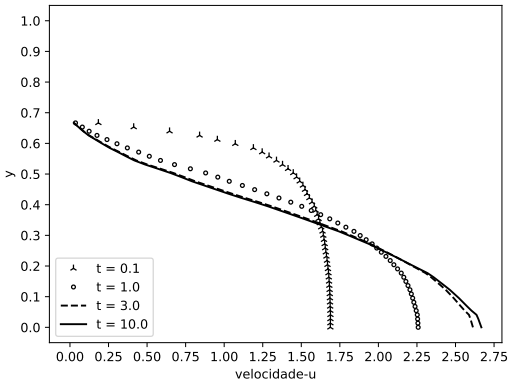

Figure 2: Velocity profile evolution.

In Figure 3, is shown the concentration evolution in time and space for half domain according to symmetry y coordinate. The evolution sequence is the top image to bottom image when the concentration field is steady state. The concentration field is represented with non-dimensional values, when the red color is $c = 1$ and blue color $c = 0$.

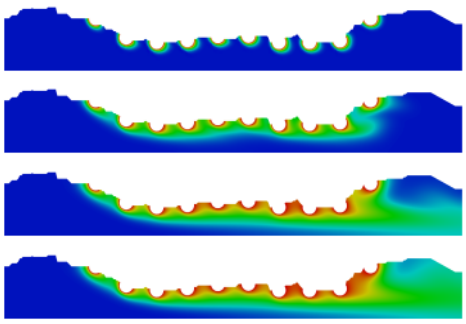

Figure 3: Concentration field evolution.

4 Conclusion

In this work, the dynamics of blood flow was shown to a coronary artery with atherosclerosis and drug-eluting stent placed and the maximum u-velocity component was nearly three times the nominal velocity. Besides, a numerial code for Navier-Stokes equation according to stream-vorticity formulation with species transport equation was developed using Finite Element Method. The Taylor-Galerkin scheme was applied to decrease the spurious oscillations as seen for moderate to high Reynolds number. The streamfunction and vorticity formulation showed an useful approximation for to calculate the velocity and concentration fields since the variables are scalars allowing then a smooth implemention.

5 Acknowledgements

The authors thank the FAPERJ (Research Support Foundation of the State of Rio de Janeiro) for its financial support.

References

[1] F. Bozsak, Chomaz J-M., and A.I. Barakat. Modeling the transport of drugs eluted from stents: physical phenomena driving drug distribution in the arterial wall. *Biomech Model Mechanobiol*, 13:327–347, 2014. doi: 10.1007/s10237-013-0546-4.

[2] J. Donea. A taylor-galerkin method for convective transporte problems. *International Journal for Numerical Methods in Engineering*, 1984.

[3] C. Geuzaine and J. Remacle. Gmsh: a three-dimensional finite element mesh generator with built-in pre- and post-processing facilities. *International Journal for Numerical Methods in Engineering*, 2009.

[4] A. Henderson. Paraview guide, a parallel visualization application. *Kitware Inc.*, 2007.

[5] W. Kessler, W. Moshage, A. Galland, D. Zink, S. Achenbach, W. Nitz, G. Laub, and K. Bachmann. Assessment of coronary blood flow in humans using phase difference mr imaging comparison with intracoronary doppler flow measurement. *International Journal of Cardiac Imaging*, 1998.

[6] H. Wang, S. McGinty, R. Lucena, J. Pontes, G. Anjos, and N. Mangiavacchi. Dynamics of blood flow in coronary artery. *International Congress of Mechanical Engineering*, 2017.

[7] W. World Health Organization. Cardiovascular diseases, 2017. URL "https://www.who.int/news-room/fact-sheets/detail/cardiovascular-diseases-(cvds)". [Online; accessed 20/11/2018 09:40].

THERMAL ANALYSIS OF HEAT SINKS ON SOLAR PANELS

Author: Lívia Corrêa[1] *livcorrea@yahoo.com.br*
Advisor(s): Daniel Chalhub[1]
[1] Rio de Janeiro State University

November 21, 2018
PPG-EM Seminars: season **2018**
www.ppg-em.uerj.br

Keywords: Thermal Analysis, Heat Sink, CITT

1 Introduction

Several researches have been studying how to enhance photovoltaic systems. The electronic components of solar panels system present high temperatures when in operation and this heat may affect the system's performance, decreasing the efficiency of PV systems, [3], and its service life time. Cooling them with cost-effetive modifications such as heat sinks may be a considered key point to minimize the electronic components temperature.

The Integral Transform Technique is a powerful method to solve differential equations based on separation of variables method. The Classical Integral Transform Technique (CITT) is an all analytical method and is most applied in linear problems, [1]. The Integral Transform Technique has been previously applied on electronic problems. For example, Corrêa and Chalhub [2] presented the solution of Solid State Electronics with one heat generation on its domain and solved by CITT.

This work proposes an analytical approach using CITT to analyze the heat transfer occurence in heat sinks applied on electronic components of solar panels.

2 Mathematical Formulation for Parallel Plate Fins

For this approach, rectangular fins were modelled on the heat sink working on steady state. The dimensionless mathematical formulation for the fin is:

$$\frac{\mathrm{d}^2\Theta}{\mathrm{d}\xi_a^2} - m^2\Theta = 0 \quad \text{for} \quad 0 \le \xi_a \le 1 \tag{1a}$$

$$\Theta(0) = 1 \qquad \left.\frac{\mathrm{d}\Theta}{\mathrm{d}\xi_a}\right|_{x=1} = -\mathrm{Bi}_a\Theta(1) \tag{1b}$$

The non-dimensional groups are defined as:

$$\xi_a = \frac{x_a}{L_a}; \quad \Theta = \frac{T - T_f}{T_b - T_f}; \tag{2}$$

$$\mathrm{Bi}_a = \frac{hL_a}{k_a}; \quad m^2 = \frac{Bi_a P_a L_a}{A_a}; \tag{3}$$

The solution for (1a) is:

$$\Theta(\xi_a) = \frac{m\cosh(m(1-\xi_a)) + Bi_a\sinh(m(1-\xi_a))}{m\cosh(m) + Bi_a\sinh(m)} \tag{4}$$

The heat transfer coefficient for the fin is:

$$h_{fin} = k_a\frac{m\,(\mathrm{Bi}_a\cosh(m) + m\sinh(m))}{m\cosh(m) + \mathrm{Bi}_a\sinh(m)}$$

3 Formulation for the base of the heat sink

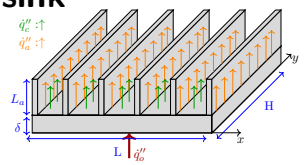

The mathematical formulation at the base of the heat sink is bidimensional, after applying a partial lumping approach for the thickness of the base, and steady-state. The nondimensionalization of the problem leads to the following mathematical formulation for $0 \le \xi \le 1$ and $0 \le \eta \le 1$:

$$\frac{\partial^2\Theta}{\partial\xi^2} + \frac{\beta^2\partial^2\Theta}{\partial\eta^2} - \mathrm{Bi}(\xi)\gamma\Theta = -Q(\xi,\eta) \tag{5}$$

$$\left.\frac{\partial\Theta}{\partial\xi}\right|_{\xi=0} = 0; \quad \left.\frac{\partial\Theta}{\partial\eta}\right|_{\eta=0} = 0; \quad \left.\frac{\partial\Theta}{\partial\xi}\right|_{\xi=1} = 0; \quad \left.\frac{\partial\Theta}{\partial\eta}\right|_{\eta=1} = 0; \tag{6}$$

The non-dimensional groups are defined as:

$$\xi = \frac{x}{L}; \quad \eta = \frac{y}{H}; \quad \Theta = \frac{T - T_f}{T_b - T_f}; \quad \beta = \frac{L}{H}; \tag{7}$$

$$\gamma = \frac{L}{\delta}; \quad \mathrm{Bi}(\xi) = \frac{h(\xi)L}{k}; \quad Q(\xi,\eta) = \frac{\dot{q}_o''L^2}{k\delta\Delta T}. \tag{8}$$

where β and γ are aspect ratios, $\mathrm{Bi}(\xi)$ is the Biot number and depends of ξ, Θ is the dimensionless temperature, ξ and η are the dimensionless versions of x and y; and Q is the heat flux acting over the domain from the chip to the base of the heat sink. The chip is located at the center of the base and the $h(\xi)$ is defined as:

$$h(\xi) = \begin{cases} h_{fin} & \text{if is in fins} \\ h_{conv} & \text{if between fins} \end{cases}$$

4 Classical Integral Transform Technique

• Solve the appropriate Helmholtz Eigenvalue Problem in cartesian coordinates.

$$\Psi_n''(\eta) + \lambda_n^2\Psi_n(\eta) = 0; \quad \Psi_n'(0) = 0; \quad \Psi_n'(1) = 0. \tag{9}$$

$$\text{Solution} = \begin{cases} \Psi_0(\eta) = 1; & \lambda_0 = 0; \\ \Psi_n(\eta) = \cos(\lambda_n \eta); & \lambda_n = n\pi; \end{cases}$$

• Define the transformation pair.

$$\text{Transformation} \quad \Rightarrow \quad \bar{\Theta}_n(\xi) = \int_0^1 \Theta \Psi_n(\eta) \mathrm{d}\eta \quad (10)$$

$$\text{Inversion} \quad \Rightarrow \quad \Theta = \sum_{n=0}^{\infty} \frac{\bar{\Theta}_n(\xi)\Psi_n(\eta)}{N_n}, \quad (11)$$

$$\text{where: } N_n = \int_0^1 \Psi_n^2 \mathrm{d}\eta \quad (12)$$

• Multiply the dimensionless diferential equation by Ψ_n and integrate in η.

• Solve the transformed equations:

For $\lambda > 0$:

$$\bar{\Theta}_n'' - (\beta^2 \lambda_n^2 + \mathrm{Bi}(\xi)\gamma)\bar{\Theta}_n = -\bar{Q}_n(\xi) \quad (13)$$

$$\bar{\Theta}_n'(0) = 0; \quad \bar{\Theta}_n'(1) = 0 \quad (14)$$

$$\text{where } \bar{Q}_n(\xi) = \int_0^1 Q(\xi, \eta)\Psi_n(\eta)\mathrm{d}\eta \quad (15)$$

For $\lambda = 0$:

$$\bar{\Theta}_0'' - (\mathrm{Bi}(\xi)\gamma)\bar{\Theta}_0 = -\bar{Q}_0(\xi) \quad (16)$$

$$\bar{\Theta}_0'(0) = 0; \quad \bar{\Theta}_0'(1) = 0 \quad (17)$$

$$\text{where } \bar{Q}_0(\xi) = \int_0^1 Q(\xi, \eta)\mathrm{d}\eta \quad (18)$$

These equations cannot be solved analytically because of the dependence of ξ on Biot number.
They are solved numerically using partial differential equation discretization with Finite Element Method using NDSolve routine on *Mathematica* software.

• Apply the inversion formula and the sum to a finite value ($n_{\max}$) until the fully convergence.

$$\text{Inversion} \quad \Rightarrow \quad \Theta = \sum_{n=0}^{\infty} \frac{\bar{\Theta}_n(\xi)\Psi_n(\eta)}{N_n} \quad (19)$$

5 Results

- Four different arrays were tested: no fin, one fin, two fins and four-fins, respectively.
- β=1, Bi(ξ)γ=0.1 for convection and Bi(ξ)γ=3 where the fins are located.
- The width for each fin is 0.1 of the length of the heat sink.
- It was used the software Mathematica.
- The routine allows the inclusion of non-regular spaced fins.

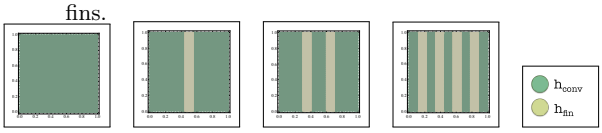

The thermal profile of the solution by CITT in all the four different layouts of heat sink is shown the the following figures.

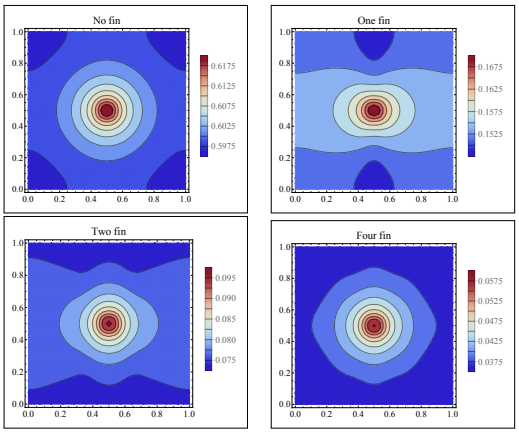

At first, it can be noticed that the isotherms curves bounds the region where the chip is located. One important detail to be noticed is also the size of the inner dark red isotherm, which presents similar dimensions as the chip. The second figure presents one fin at the center of the heat sink and the increase of the heat dissipation on the region of the fin is noticed by the darker blue stains exactly where the fin is found. The size of the inner dark red isotherm is smaller, indicating a more intense heat dissipation. Also, all the heat sink presents lower temperatures in comparison with the previous case without fins.

The solution for the two-fin case has a visual expressive reduction of temperature where the fins are located. Also, the inner dark red isotherm is smaller, the heat sink presents lower temperatures from the previous cases, the maximum temperature on this heat sink does not achieve 0.1. Finally, the four-fin layout heat sink is shown in last figure. Because this layout present equally spaced fins in all the extension of the heat sink, the thermal profile of this case resemble with the no-fin case. However, the inner dark red isotherm is reduced to a small point on the profile and maximum temperature at the heat sink is reduced from 0.619608, of the no-fin case, to 0.0576527. This four-fin case is, then, the most efficient heat sink layout shown in this work, dissipating more heat and reducing the temperature for lower values.

6 Conclusions

- CITT had a great performance to obtain high accuracy solutions.
- The ξ dependence on Biot made unworkable the achievement of an analytical solution for the base of the heat sink. The Finite Element Method numerical discretization solved the transformed differential equations.
- The increase of the number of fins increase the heat dissipation, reducing the temperature.
- This is a preliminary work. In the future, a bidimensional fin formulation solution will be proposed.

7 Acknowledgments

The authors thank to FAPERJ for the Financial Support.

References

[1] D J N M Chalhub, L A Sphaier, and L S de B Alves. Semi-analytical method for the solution of the poisson equation derived from the navier-stokes using integral transform. In *ASME 2014 12th International Conference on Nanochannels, Microchannels and Minichannels collocated with the ASME 2014 4th Joint US-European Fluids Engineering Division Summer Meeting*, 2014.

[2] L M Corrêa and D J N M Chalhub. Solution of the heat conduction in solid-state electronics by integral transforms. In *24th ABCM International Congress of Mechanical Engineering*, 2017.

[3] P M Cuce and E Cuce. A novel model of photovoltaic modules for parameter estimation and thermodynamic assessment. *International Journal of Low-Carbon Technologies 7, 159-165*, 2012.

CHARACTERIZATION OF NANOCOMPOSITS (PLA / HDPE-G-AM / HDPE-GREEN / N-CACO3)

Author: Camilla Fonseca Morgado[1] *millafff@gmail.com*
Advisor(s): Marilia Diniz[1]
[1] State University of Rio de Janeiro

PPG-EM Seminars: season **2019**
www.ppg-em.uerj.br
Jan 09, 2019

Keywords: PLA, HDPE, Characterization techniques, Polarized Light

1 Introduction

Some biopolymers have great potential for replacing, in certain applications, polymers from fossil sources. Despite all the advantages, biopolymers have some technical limitations. Thus, many research groups have been dedicated to the study of the modification of the biopolymers to enable the processing and use of the same in several applications. For this, blends, composites, nanocomposites, have been studied in order to improve properties such as processability, thermal resistance, mechanical properties, rheological properties, gas permeability and degradation rate. [1,2]

2 Materials And Methods

The production of these PLA / HDPE-g-AM / HDPE-GREEN / n-CaCO3 nanocomposites occurred through different proportions of mixtures of PLA and polyethylene from renewable source (HDPE-Green), made possible by the action of the compatibilizing agent grafted polyethylene maleic anhydride (HDPE-g-AM) and the nanoparticulate calcium carbonate additive (n-CaCO3). These materials were obtained by the polymer research group of the State University of Rio de Janeiro. [2] Table 1 shows the mixtures tested.

Mixture	PLA (%)	n-$CaCO_3$ (%)
EXP 01	7	4
EXP 02	28	1
EXP 03	7	1
EXP 04	28	1
EXP 05	28	4
PLA (puro)	-	-
HDPE (puro)	-	-

Table 1: Composition (in percent) by weight used to make test specimens. Pure PLA and HDPE. [2]

Samples were cut in the longitudinal and transverse direction of lamination of the 6 m thick composites, for each condition tested, on a microtome of the RWC mark MT 990. The fine samples were fixed in coverslots and observed through a polarized light optical microscope of the Brand ZEISS AxioImager M2m with digital system for acquisition of images. Light field images were generated at zero degree and at 75 degrees of polarization angle for each pair of fine samples (longitudinal and transverse). Samples in the transverse and longitudinal direction of lamination of the specimens were cut and embedded in cold cure resin and then underwent a preparation process in which the exposed surfaces were polished with diamond pastes in the particle sizes 6, 3, 1 and of m, respectively. Vickers (HV) microhardness measurements for each condition were obtained by means of a Pantech MV-1000A microdurometer with 10g load and a time of 15 seconds of application. Five indentations were performed for each test body / longitudinal / transverse direction.

3 Results and Discussion

Images were generated in pairs (zero degree and 75 degrees) with the following correspondence: everything that was in dark tonality in an image that inverted its tonality becoming clear in the corresponding pair image, had as meaning a region that polarized the light, that is , showed a crystalline region or some degree of crystallinity (preferred orientation). [4] Figures 1 and 2 show examples of polarized light images generated in pairs for the fine samples of all conditions tested. It was observed that for the conditions of Experiments 2, 4 and 5, both in the longitudinal direction and in the transverse direction of rolling, there were crystalline regions, in some places with some preferential orientation, in others with a "tangled", probably due to the existence of superposed layers of crystalline regions in the fine sample. For experiments 1, 3, pure HDPE and pure PLA, it was observed that there was no inversion of colors / shades.

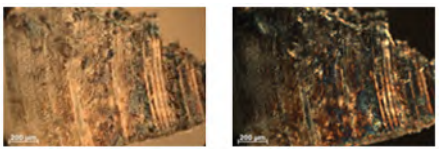

Figure 1: Fine samples under polarized light for conditions EXP 01 - LONGITUDINAL - 100X magnification - zero degree par - 75 degrees polarization

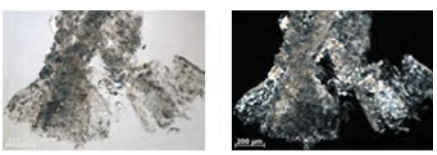

Figure 2: Fine samples under polarized light for conditions EXP 02 - LONGITUDINAL - 100X magnification - zero degree par - 75 degrees polarization

Table 2 presents the Vickers microhardness results for each condition tested. The conditions 2 and 4 showed a tendency of greater hardness between the blends and both had 28 percent of PLA and 1 percent of CaCO3, besides having presented with some degree of crystallinity. However, the formulations 1 and 3 that had 7 percent of PLA showed lower hardness and no crystallinity when compared to conditions 3 and 7. Thus, the results suggest that although the hardness of the composites is close to the matrix value, there is evidence that dispersed phase (PLA) had influence on the hardness and the crystallinity of the mixtures.

LONGITUDINAL							
	EXP1	EXP2	EXP3	EXP4	EXP5	PLA	HDPE
MEDIA	7,636	10,036	8,024	9,753	8,570	17,986	7,947
DESV. PAD	0,687	1,226	0,739	1,537	0,797	0,792	0,813
TRANSVERSAL							
	EXP1	EXP2	EXP3	EXP4	EXP5	PLA	HDPE
MEDIA	7,731	8,965	7,405	9,304	8,311	18,937	8,233
DESV. PAD	0,879	1,064	0,823	0,938	0,703	1,125	0,385

Table 2: HV microhardness values for each condition tested: longitudinal section (LONG) and transversal (TRANS) of lamination of the composites

4 Conclusions

The qualitative analysis of the images obtained by polarized light suggests that the experiments with the highest PLA content were those with the highest color inversion (light / dark) and, therefore, a higher degree of crystallinity. The results of the hardness measurements showed that experiments 2 and 4, which had higher amounts of PLA (28 percent), had higher hardness values. Although the hardness of the composites is close to the matrix value (HDPE), there is an indication that the dispersed phase (PLA) had an influence on the hardness.

References

[1] G. F. Brito*, P. Agrawal, E. M. Araújo, T. J. A. Mélo - Biopolímeros, Polímeros Biodegradáveis e Polímeros Verdes - Revista Eletrônica de Materiais e Processos, v.6.2, 2011

[2] Oliveira, Amanda Gerhardt de. - Desenvolvimento e avaliação de nanocompósitos à base de polietileno de alta densidade (HDPE-Verde)/poliácido lático - PLA e nanocarbonato de cálcio para fábricação de embalagens- Dissertação de mestrado - Universidade do Estado do Rio de Janeiro- 2015

[3] P. Robinson and M. Davidson, “Introduction to Polarized Light Microscopy,” 2015. Online. Available: http://www.microscopyu.com/. Acessado: 19-ju-2018.

[4] Metals Handbook - Light Microscopy e Polarized light - 2004.

MODELING AND OPTIMIZING A VEHICLE SUSPENSION CONSIDERING USER SAFETY AND COMFORT IN AN IRREGULAR (RANDOM) ROAD PROFILE

Author: Julio Basilio[1] *juliobasilio@ymail.com*
Advisor(s): Jose Telles ; Francisco Soeiro[1]
[1] State University of Rio de Janeiro

PPG-EM Seminars: season **2018**
www.ppg-em.uerj.br
January 16, 2019

Keywords: Suspension, Road Profile, QCM.

1 Introduction

Suspensions are extremely important components for vehicles, regardless of their use, from the transport of people to the transport of loads. Its are responsible for reducing the impact of runway irregularities to your users and other vehicle components, as well as improving ride stability and driveability. In essence, the suspension acts directly to guarantee comfort and safety to the user, characteristics that are conflicting when we try to improve them in the same time. While the use of a "stiffer" suspension to improve stability, where the corrugations and runway holes will not be filtered by the stiffer spring, it compromises the comfort of the user. A suspension commonly called "softer", to improve comfort, can compromise the stability of the car, especially in curves. Already in sudden braking, a very soft set in the front can cause the car dive too much.

2 Methodology

2.1 Comfort Criteria

According to [4], comfort is linked to human perception of the vibrations originating from the system. Experiments related to ergonomics show that this perception of vibrations depends on vertical acceleration.

The standard [1], which presents general requirements on mechanical vibration and human exposure, establishes comfort indexes as a function of acceleration. Acceleration values less than 0.315 m/s^2 are considered comfortable, since values greater than 2 m/s^2 are seen as extremely uncomfortable.

In addition, according to [5], the human body has a natural vibration. This implies that if an external frequency coincides with the natural frequency of the system, resonance and amplification of the movement occurs. A vertical excitation between 4 and 8 Hz for example, is perceived as very unpleasant because it is the resonance frequency of the region of the abdomen.

2.2 Safety Criteria

The load on the wheel f_{Wheel} is one of the criteria for driving safety, consisting of the static force f_{Stat}, originating from the mass of the vehicle (mass suspended) and the dynamic force $f_{(Dym,crit)}$ generated by vehicle vibration.

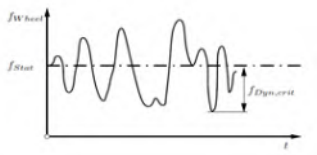

Figure 1: Static force f_{Stat} and dynamic $f_{(Dym,crit)}$

As presented by Fig. 1, the more negative the dynamic force in relation to the static force, the lower the safety in driving. From this, [4] have proposed $R = \frac{f_{Stat} - f_{(Dym,crit)}}{f_{Stat}}$, where R represents the safety margin between the dynamic and static forces. According to them, even in the worst case (irregular road, front wheel, maximum speed), the safety margin R ≈ 0.75 indicates a safe trip.

2.3 Mathematical Model

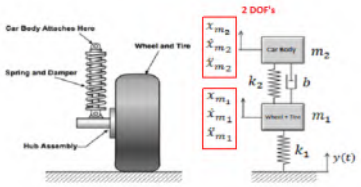

Figure 2: The model simplified of quarter car model

The scheme shown in Fig. 2, represents quarter car model (QCM) with 2 (two) degrees of freedom (DOF) used to obtain the mathematical model of the study.

From this model with 2 DOF's, using the differential equations of forces, according to the free body diagram of the mass of the car (sprung mass) and the wheel (unsprung mass), the mathematical model was found

in the form of equation state, shown in Eq. (1).

$$\begin{vmatrix} x_{m1} \\ \dot{x}_{m1} \\ x_{m2} \\ \dot{x}_{m2} \end{vmatrix} = \begin{vmatrix} 0 & 1 & 0 & 0 \\ -\frac{k_1+k_2}{m_1} & -\frac{b}{m_1} & \frac{k_2}{m_1} & \frac{b}{m_1} \\ 0 & 0 & 0 & 1 \\ \frac{k_2}{m_2} & \frac{b}{m_2} & -\frac{k_2}{m_2} & -\frac{b}{m_2} \end{vmatrix} \begin{vmatrix} x_{m1} \\ \dot{x}_{m1} \\ x_{m2} \\ \dot{x}_{m2} \end{vmatrix} + \begin{vmatrix} 0 \\ \frac{k_1}{m_1} \\ 0 \\ 0 \end{vmatrix} y(t) \quad (1)$$

$$\begin{vmatrix} \ddot{x}_{m2} \\ f_{dyn} \end{vmatrix} = \begin{vmatrix} \frac{k_2}{m_2} & \frac{b}{m_2} & -\frac{k_2}{m_2} & -\frac{b}{m_2} \\ -(k_1+k_2) & -b & k_2 & b \end{vmatrix} \begin{vmatrix} x_{m1} \\ \dot{x}_{m1} \\ x_{m2} \\ \dot{x}_{m2} \end{vmatrix} + \begin{vmatrix} 0 \\ k_1 \end{vmatrix} y(t)$$

However, the model used in the simulations will be in function of the system parameters, system damping coefficient ξ and natural frequency not damped f_n, to facilitate the restrictions imposed by the comfort and safety criteria. As also considered the sprung mass (m_2) equal to 189.5 kg, unsprung mass (m_1) equal to 20 Kg and the tire stiffness (k_1) equal to 100.000 N/m.

2.4 Input Data (Road Profile)

For MATLAB simulations and system behavior analysis, it is necessary to define an input to the system. Based on this, and aiming at results consistent with reality, a mathematical model representing classes of road profiles was used. From the [2], which describes methodologies to be used for generating the road surface profile, [3] proposed a stochastic representation of the mathematical model shown in Eq. (2), and a classification of the roads according to the constant K. Where, K values equal to 3 is very good quality roads to good , and goes to the K value equal to 6, which is bad roads to very bad.

$$h(x) = \sum_{i=0}^{N} \sqrt{\Delta n}.2^K.0,001.(\frac{n_0}{i.\Delta n}).\cos(2.\pi.i.\Delta n.x + \varphi_i) \quad (2)$$

3 Results

Once the system has been defined and its input, we can analyze the behavior of the suspension in a medium road, medium grade (Class B) to bad (Class C), with constant K equal to 4. Such analysis was performed using MATLAB for make the simulations and obtain the 2D and 3D graphs, comparing the outputs of the system, vertical acceleration of the chassis $\ddot{x}_{m2}$ and dynamic force on the wheel f_{dyn}, to the parameters of the system: natural frequency not damped and damping coefficient. In both system responses their effective values (RMS) are obtained.

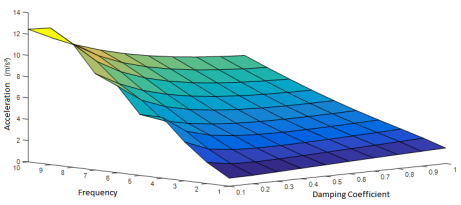

Figure 3: 3D graphics Acceleration RMS

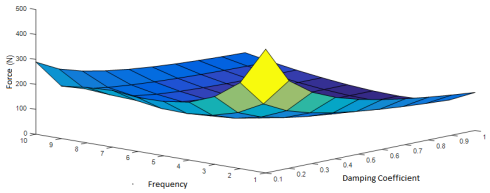

Figure 4: 3D graphics Force RMS (f_{dyn})

The Figs. **??** e 4 illustrate the problem initially exposed, while high natural frequency values result in a greater acceleration ($\ddot{x}_{m2}$), and consequently, worse comfort. The Dynamic Force on the wheel (f_{dyn}) decreases the higher the frequency, so the safety improves.

4 Conclusion

The results of the simulations in MATLAB, confirm the need to use optimization methods to find optimal values for the suspension parameters. Since we have more than one goal, which is comfort and safety, we should seek multiobjective optimization methods. Among the methods currently developed, the one that presented the most ideal study is Goal Attaintment Method, mainly because it is present in the MATLAB Toolbox. This study provides the project variables (ξ e f_n), some constraints and goals (Eqs. (3) and (4)), and functions objectives, as obtained in Eq. (1) . Thus, to obtain the optimal values of the parameters of the suspension enough to develop the development of the optimization method. It is worth remembering that for optimization it will be necessary to define "weights" for the objectives.

$$1 \leq f_n < 4 = \begin{cases} 0.75 \leq \ddot{x}_{m2} \leq 5m/s^2 \\ 90 \leq f_{dyn} \leq 500N \end{cases} \quad (3)$$

$$R = \frac{f_{Stat} - f_{Dyn}}{f_{Stat}} < 0,75 = \begin{cases} f_{Dyn} \leq Weight * 0,25 \\ f_{Dyn} \leq 473,75N \end{cases} \quad (4)$$

References

[1] ISO International Standard 2631. Mechanical vibration and shock – evolution of human exposure of whole – body vibration: General requirements. Beuth, Berlin, 1997-2004).

[2] ISO International Standard 8608. Mechanical vibration - road surface profiles - reporting of measured data. Geneva, Switzerland, 2016.

[3] D. Ciampa, M. Agostinacchio, and S. Olita. The vibrations induced by surface irregularities in road pavements - a matlab approach. *European Transport Research Review*, 1:267–275, 2013.

[4] Karl Poop and Werner Schiehlen. *Ground Vehicle Dynamics*. Springer, 1993.

[5] Antonio Carlos Vendrame. Vibrações ocupacionais. www.higieneocupacional.com.br, 2005.

CHARACTERIZATION OF MECHANICAL AND SURFACE FINISHING PROPERTIES OF METALLIC COATING OBTAINED BY ELECTRIC ARC THERMAL SPRAY

Author: Pamella Kesseler de Campos[1] *pamella.kesseler@gmail.com*
Advisor(s): Marília Garcia Diniz[1]
[1] State University of Rio de Janeiro

PPG-EM Seminars: season **2019**
Jan 16, 2019 www.ppg-em.uerj.br

Keywords: Erosion, Metallic Coating, Thermal Spraying.

1 Introduction

The national production of electric energy is mostly from the hydroelectric and thermoelectric sector [1]. Brazilian thermoelectric plants that use coal as a thermal source use pulverized combustion technology. Considering the high percentage of ash present in Brazilian coal, the metallic parts of the interior of the boiler, and especially the pipes inside the boiler, suffer accentuated wear depending on the composition and amount of ash that can lead to losses for profit to the operator. In this sense it is essential to delay the deterioration process of the tubes surface . There are several processes that can be used industrially to increase surface properties by delaying the pipes deterioration and devices inside the boilers, obtaining greater hardness, improving the wear resistance, corrosion, high temperatures resistance, maintaining the electrical or thermal conductivity between other requirements. Among the processes, we can mention thermal spraying, in which a substance or a combination of them fuse (in their conventional options) through the use of some kind of energy (combustion, electric arc, plasma, among the most common) and then this substance is projected toward a previously prepared surface with a suitable roughness, which will help to get a better grip of the designed material. The sprinkled material is intended to provide the base metal with the desired property to combat or delay the deterioration process of the surface thereof.

2 Objective

The aim of this work was to characterize some properties of a metallic coating in order to protect the surface of the boiler piping of thermoelectric power plants against the aggressive action of the ash from coal burning. The evaluated parameters considerably influence the characteristics of the service life of the coatings [2]. At this stage of the research, Vickers (HV) and medium roughness (Ra) microhardness measurements of the surface of the coating were tested.

3 Material and Method

In this experiment, an 8 mm thick steel sheet donated by Arcellor Mittal with a chemical composition and thickness similar to the steels used in the water wall pipes of Brazilian boilers (0.2 porcent C) was used. As a coating to be studied, a metal alloy, referenced herein as Alloy B, was used. Table 1 shows the chemical composition of the alloy used.

Chemical Composition	
Element	**Weight %**
Silicon	1,6
Chromium	29
Manganese	1,65
Boron	3,75
Iron	Balance

Table 1: Alloy's B composition

The TAFA - 8835 thermal spray equipment was used at a pressure of 60 Psi, Amperage - 100, Voltage – 28 - 30 V and compressed air to propel the particles to the substrate. Spraying was performed perpendicularly (90o 5o) in Horizontal and Vertical passes with stipulated sprinkling distance between 80 - 120 mm on the surface of the previously prepared sample (Sa 2 1/2 abrasive blasting). After spraying the final thickness of the sample was approximately 8.7mm. Hardness measurements were performed in three different regions of the surface of the coating and in three substrate regions of a sample previously submitted to metallographic preparation, in a total of 6 grids of 30 points each. Roughness measurements were performed through Digital Image Processing (PDI) obtained by Optical Microscopy (OM) and through a roughness gauge of the Digital Surface Profile Gauge | Elcometer 223 - Elcometer USA.

4 Results and Discussion

Table 2 presents the results of the hardness tests. It was observed that the hardness of the coating was on the order of four times greater than the hardness of the substrate to be protected. This property was homogeneous for the coated layer.

	Grind 1 (HV)	Grind 2 (HV)	Grind 3 (HV)	Avarege (HV)
Coating	753,29	754,71	683,61	730,54
Coating and substrate edge	217,7	223,6	212,06	217,79
Substrate				179,26

Table 2: Hardness test results.

The homogeneity of the hardness values indicates that good adhesion of the cast particles of the coating occurred and that the spray distance proved to be effective for the intended purpose, since this parameter is a determinant factor for a desired hardness increase [3]. Table 3 presents the results of average roughness (Ra) of the sprinkled surface for the two methods used.

Roughness (µm)	
PDI	27,49
Rugosimeter	247,84

Table 3: Sample sprinkled surface roughness.

The result of the roughness test by means of the PDI was very dissimilar to the result obtained by means of the rugosimeter. This may be related to the fact that the PDI technique did not consider the effect of curvature on a macroscopic scale of the surface of the material, but only the relative microscopic scale. The PDI results were not coherent, unlike the values obtained by the rugosimeter measurements that were close to the values normally generated by the electric arc thermal sprinkling technique.

5 Conclusions

- The coating parameters allowed a deposit homogeneously on the surface of the sample;
- The hardness of the coating was approximately 4x greater than that of the substrate;
- Roughness measurements by PDI differed significantly from the measurements obtained with the rugosimeter, the latter being the method that still remains the most reliable.

References

[1] Associação Brasileira dos Distribuidores de Energia Elétrica – ABRADEE. Visão geral do setor elétrico. Disponível em http://abradee.com.br/setor-eletrico/visao-geral-do-setor. Acessado em 30/05/2016.

[2] Developing empirical relationship to predict hardness in WC-10Co-4CrHVOF sprayed coatings. K. Murugan. Science Direct, 2014. Pages 1-10.

[3] Coating parameters influence on mechanical properties of coatings. Ihsan Kucukrendeci. Journal of applied sciences, 2013. Pages 1-6.